Hybrid acoustic materials through assembly of tubes and microchannels : Design and experimental investigation

Josué Costa-Baptista

(Department of Mechanical Engineering, Laboratory for Acoustics and Vibration Analysis (LAVA), Polytechnique Montréal, Montréal, Canada and Department of Mechanical Engineering, Laboratory for Multiscale Mechanics (LM2), Polytechnique Montréal, Montréal, Canada)

Edith Roland Fotsing

(Department of Mechanical Engineering, Laboratory for Acoustics and Vibration Analysis (LAVA), Polytechnique Montréal, Montréal, Canada and Department of Mechanical Engineering, Research Center for High Performance Polymer and Composite Systems (CREPEC), McGill University, Montréal, Canada)

Jacky Mardjono

(Safran Aircraft Engines, Villaroche, Rond Point René Ravaud – Réau, Moisy-Cramayel Cedex, France)

Daniel Therriault

(Department of Mechanical Engineering, Laboratory for Multiscale Mechanics (LM2), Polytechnique Montréal, Montréal, Canada and Department of Mechanical Engineering, Research Center for High Performance Polymer and Composite Systems (CREPEC), McGill University, Montréal, Canada)

Annie Ross

(Department of Mechanical Engineering, Laboratory for Acoustics and Vibration Analysis (LAVA), Polytechnique Montréal, Montréal, Canada and Department of Mechanical Engineering, Research Center for High Performance Polymer and Composite Systems (CREPEC), McGill University, Montréal, Canada)

Structured abstract:

Purpose:

The design and experimental investigation of compact hybrid sound absorbing materials presenting low frequency and broadband sound absorption.

Design/methodology/approach:

The hybrid materials combine microchannels and helical tubes. Microchannels provide broadband sound absorption in the middle frequency range. Helical tubes provide low frequency absorption. Optimal configurations of microchannels are used and analytical equations are developed to guide the design of the helical tubes. Nine hybrid materials with 30 mm thickness are produced via additive manufacturing. They are combinations of one-, two- and four-layer microchannels and helical tubes with 110 mm, 151 mm and 250 mm length. The sound absorption coefficient of the hybrid materials is measured using an impedance tube.

Findings:

The type of microchannels (i.e., one, two or four layers), the number of rotations and the number of tubes are key parameters affecting the acoustic performance. For instance, in the 500 Hz octave band (α_{500}), sound absorption of a 30 mm thick hybrid material can reach 0.52 which is 5.7 times higher than the α_{500} of a typical periodic porous material with the same thickness. Moreover, the broadband sound absorption for mid-frequencies is reasonably high with and $\alpha_{1000} > 0.7$. The ratio of first absorption peak wavelength to structure thickness λ/T can reach 17, which is characteristic of deep-subwavelength behaviour.

Originality:

The concept and experimental validation of a compact hybrid material combining a periodic porous structure such as microchannels and long helical tubes are original. The ability to increase low frequency sound absorption at constant depth is an asset for applications where volume and weight are constraints.

Keywords: sound absorbing materials, design, additive manufacturing, low frequency, subwavelength absorption, deep-subwavelength absorption

Introduction

Additive manufacturing (AM), as a family of processes, allow the creation of structures with unusual and complex shapes that would hardly be possible with traditional fabrication techniques [1–4]. Parts with improved functional performance are designed for specific applications. For instance, topology optimization – a technique used to optimize the design of structures in within a given volume and under specific loads, boundary conditions and constraints – and three-dimensional (3D) printing are used to produce lightweight parts in the aerospace, automotive and medical industries [5–7]. Similar techniques are employed to design and fabricate periodic porous structures (PPS) for noise control purposes.

PPS are a class of sound absorbing materials made of the periodic arrangement of unit cells with well-defined geometrical parameters (e.g., pore size and wall thickness) [8,9]. Micro-lattices [8,10,11], microchannels [12,13], sonic crystals [14], micro-helix metamaterials [15] and triply periodic minimal surfaces (TPMS) [16] are examples of effective sound absorbing PPS obtained via 3D printing. These materials can exhibit broadband absorption at frequencies lower than the quarter-wave resonance frequency (QWRF $= c/4T$, where c is the sound speed and T is the material thickness) [8,11–13]. The first absorption peak of 30 mm thick uniform microchannels and micro-lattices can occur around 2250 Hz [10,13] (i.e., 583 Hz below the QWRF). However, it remains challenging to achieve low frequency absorption (below 1000 Hz) unless thick structures are used, which is prohibitive in many applications due to space constraints. Additional challenges come from the ability to produce PPS with pore size in the sub-millimeter or micrometer ranges.

The stacking of PPS with different geometrical parameters in multilayered or graded materials is an efficient way to improved subwavelength absorption [11,12]. For example, the first absorption peak of multilayered microchannels and graded micro-lattices are ~ 1650 Hz (i.e., a 600 Hz improvement over the one layer structures and 1183 Hz below the QWRF) [11]. Folded or coiled tubes can work as acoustic resonators [17–19] and are interesting concepts to improve low frequency absorption. For instance, broadband quasi-perfect sound absorption between 1150 Hz and 2000 Hz was achieved with a folded metaporous material [20]. Despite the remarkable improvement of 1100 Hz over the uniform PPS and 500 Hz over the multilayered or graded periodic porous structures, achieving low frequency absorption (below 2000 Hz) while keeping a reasonable absorption in mid frequency range (2000-4000 Hz) is still a challenge for periodic porous structures.

The purpose of this work is to create hybrid sound absorbing materials capable of absorbing low and mid frequency noise. The hybrid materials are created by assembling microchannels and coiled tubes,

both produced via fused filament fabrication (FFF) method. Their micro-structure is assessed by microscopy observation and their sound absorption coefficient is measured using an impedance tube. The sound absorption of the different structures is analysed and compared to determine materials with best low frequency sound absorption. The developed hybrid materials exhibit deep-subwavelength behavior and broadband sound absorption.

Design of the hybrid material

The developed hybrid materials are made by the assembly of microchannels and helical tubes. The idea of assembling microchannels and coiled tubes is to create hybrid materials in which each constitutive part would contribute to the absorption in different frequency ranges. The microchannels provide broadband sound absorption for middle frequency range [13] while the helical tubes provide the low frequency absorption.

Microchannels can be defined as a network of long parallel perforations which are not interconnected and non obstructed. As an example, Figure 1a-c shows schematics of optimal microchannels with 1, 2 and 4 layers, respectively. Longitudinal cuts of a section slightly larger than the greatest channels (layers 2 and 4) are shown to explain the concept with a compact illustration. The same section of the concept can be extended to materials occupying a larger surface. T is the total thickness of the acoustic material (the sum of t_n) where t_n is the thickness of a specific layer. The geometrical parameters of one layer of channels are presented in Figure 1d. D is the channels size; W is the wall thickness; P is the mesh pitch ($P = D + W$); and t is the thickness of the layer.

Table I lists the optimal channel sizes and layer thicknesses of the 1, 2 and 4 layers microchannels. The optimal parameters are obtained via microstructure and sound absorption optimization. The sound absorption coefficient of microchannels is simulated with the Johnson-Champoux-Allard-Lafarge (JCAL) model [21–23] and the transfer matrix method (TMM) [24,25]. The JCAL parameters are numerically evaluated using the Two-scale Asymptotic Method (TAM) solved with the Finite Element Method (FEM) implemented in Comsol Multiphysics 5.4 [26]. The simplex Nelder-Mead optimization method [27,28] is used to find the size of the channels and the stacking sequence leading to the best acoustic absorption in

Table I. For the sake of conciseness, theory and details of the acoustic modelling and optimization of microchannels are not presented but can be found in [12,13]. It is shown that with the proper density, microchannels can present broadband acoustic absorption similar or higher than that of stochastic porous materials [13]. Moreover, the microchannels offer a good compromise between effective acoustic properties and useful mechanical properties compared to other 3D printed acoustic structures and can be considered as viable candidates for applications where structural resistance is required [29]. Figure 1e shows the sound absorption coefficient of optimal microchannels with 30 mm thickness and 1, 2 and 4 layers. Optimal microchannels features broadband sound absorption with the first resonance frequency below the quarter wave resonance frequency of traditional porous materials, QWRF = 2833 Hz (i.e., $f = c/4T$ for c = 340 mm/s and T = 30 mm). The first resonance frequency of the 1 layer microchannels is 2250 Hz. The first resonance frequency of the 2 and 4 layers materials is around 1900 Hz, allowing higher absorption at low frequencies (i.e. below 2000 Hz). The second resonance frequency of the 4 layers microchannels is 5150 Hz. Moreover, 2 and 4 layers microchannels exhibit broadband absorption over a large frequency range. However, from Figure 1e, it can be observed that the absorption coefficient of 1, 2 and 4 layers microchannels remains low ($\alpha < 0.6$) below 1000 Hz (grey area).

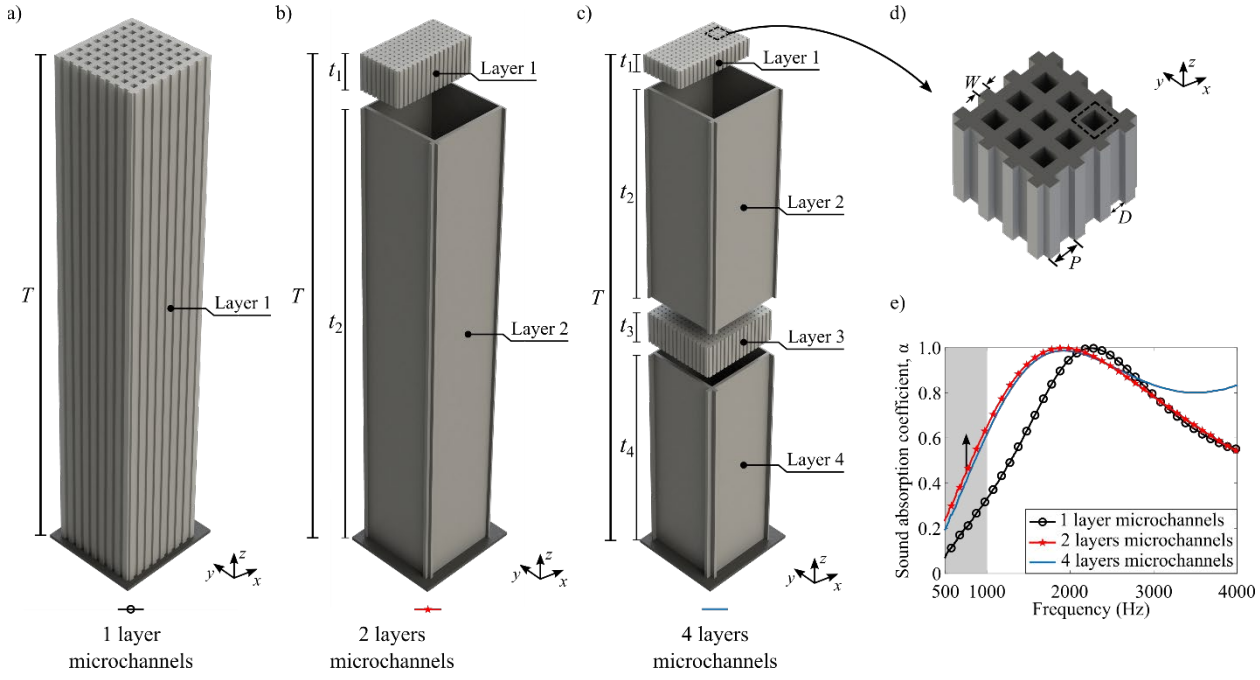

Figure 1 – Design of the hybrid materials: a-c) are schematics of microchannels with, 1, 2 and 4 layers, respectively; d) parameters of one layer of channels; e) Experimental sound absorption coefficient of 1, 2 and 4 layers microchannels.

Table I - Channel sizes and layer thicknesses of microchannels 1, 2 and 4 layers

1 layer		**2 layers**		**4 layers**	
Channel size	Layer thickness	Layer thickness	Channels size	Layer thickness	Channel size
T = 30 mm	D = 290 μm	t_1 = 2 mm	D_1 = 100 μm	t_1 = 1 mm	D_1 = 100 μm
				t_2 = 13 mm	D_2 = 4.6 mm
		t_2 = 28 mm	D_2 = 4.6 mm	t_3 = 2 mm	D_3 = 100 μm
				t_4 = 14 mm	D_4 = 4.6 mm

When properly designed, tubes can lead to narrowband acoustic absorption at frequency centered at the quarter-wave resonance. Moreover, by increasing the length of the tubes, the resonance is shifted towards lower frequencies ($f \propto \frac{c}{4L}$, where L is the length of the tube) [30]. Therefore, when assembled properly, long straight tubes would improve the low frequency absorption of microchannels or any porous material. However, the increased thicknesses would make the solution impractical. Coiling is an effective technique to contain long tubes in small volumes. It is proven that the helical conformation is the most efficient way to fold a tube. Indeed, the helical conformation maximizes entropy, and therefore provides compact and structurally stable tubes [31–34]. This shape is observed in DNA [33,34], heat exchangers [35], stairs [36], rods and springs [37], for example. In the case of acoustic resonators, the helical tubes would provide a smooth and continuous guide for the sound waves to be trapped and dissipated [20]. Consequently, the combination of microchannels and helical tubes may lead to a compact material with improved low frequency and broadband acoustic absorption.

Figure 2 shows the parameters of the helical tubes on the hybrid materials. T is the hybrid material total thickness, R_h is the helix radius, R_t is the tubes radius, W_t is the tubes wall width, H_h is the helix height and E is the elbow height. H_h = 28 mm and T = 30 mm, therefore E = 2 mm ($E = T - H_h$). The elbow functions are to align the tube entrance with the incident wave propagation direction and to provide a smooth transition to the helix. The length of the tubes L is calculated as follows:

$$L = \sqrt{C^2 + H_h^2} + 2.66 \text{ mm}, \tag{1}$$

where $C = \xi(2\pi R_h)$ is the circumference of the helix and 2.66 mm is the theoretical elbow length. The length of the tubes L, and therefore the absorption peak frequency or resonant frequency ($f \sim c/4L$), is directly related to the volume of the hybrid material sample. Larger samples can be used to increase the tubes length lowering the resonant frequency. The helix radius R_h is calculated using the following equation:

$$R_h = R_s - R_t - W_t. \tag{2}$$

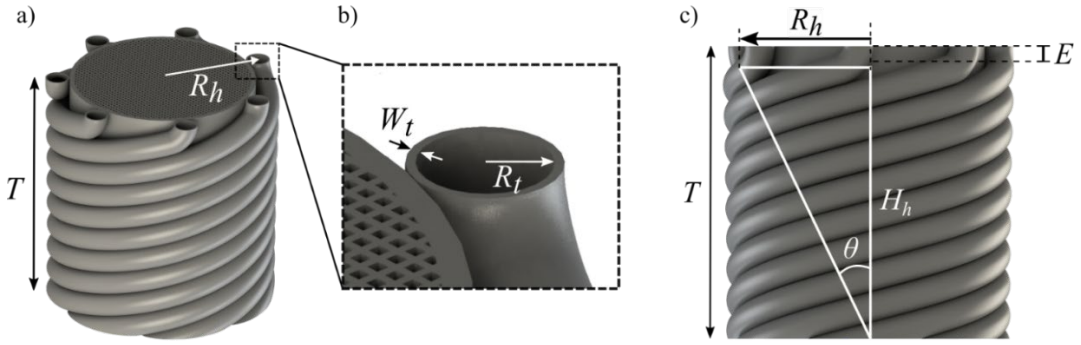

Figure 2 – Geometrical parameters of the helical tubes in the hybrid materials: a) general schematic view of the hybrid material; b) detail of a tube entrance; c) front view of the hybrid material.

The geometrical parameters are adjusted to avoid tubes overlapping. For a given helical tube's configuration (ξ, H_h, R_t and W_t), the maximum number of tubes is calculated with the following relation:

$$N \approx \frac{H_h}{\xi \cos\theta \, 2(R_t + W_t)}, \tag{3}$$

where $\theta = \arctan\left(\frac{R_h}{H_h}\right)$. The calculated N is rounded to the lower integer because the number of tubes cannot be fractionated. Rounding up is not an option because tubes would overlap. Maximizing the number of tubes for a given configuration is important to increase the dissipation on the absorption frequency.

Hybrid materials with three different number of rotations and, consequently, different number of tubes are investigated in this work. Figure 3 presents different configurations of the hybrid material made by microchannels cinctured by helical tubes. N is the number of tubes, ξ is the number of rotations of the helix. Their parameters are listed in Table II. Increasing ξ aims at expanding the length of the tubes and consequently lower the absorption frequency. For instance, ξ = 1.25 leads to L = 110 mm (3.7 times the hybrid material thickness T), ξ = 1.75 leads to L = 151 mm (5 times T) and ξ = 2.95 leads to L = 250 mm (8.3 times T). The characteristics of the microchannels in the centre are shown in

Table I.

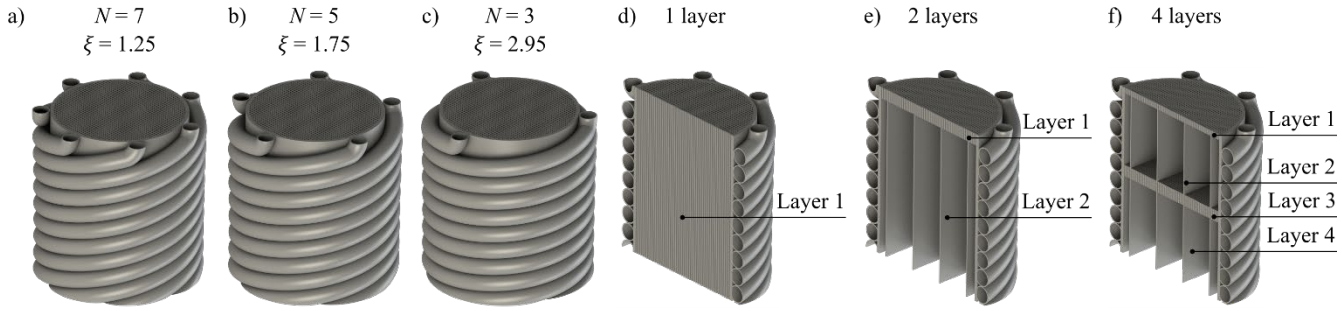

Figure 3 – Schematics of different configurations of the hybrid material : a) to c) hybrid material with 7, 5 and 3 coiled tubes, respectively. d) to f) hybrid material with different 1, 2 and 4 layers microchannels, respectively.

Table II – Parameters of the helical tubes for the hybrid materials

Sample radius, R_s	**Tube radius, R_t**	**Tubes wall width, W_t**	**Helix radius, R_h (Eq. (2))**	**Number of rotations (ξ)**	**Number of tubes, N (Eq. (3))**	**Tube length L (Eq. (1))**
15 mm	1.35 mm	0.4 mm	13.25 mm	1.25	7	110 mm
				1.75	5	151 mm
				2.95	3	250 mm

Experimental methods

Manufacturing

The coiled tubes and microchannels are produced separately using the Black and Red Raise3D® premium polylactic acid (PLA), respectively. The Raise 3D Pro2 FFF 3D printer with filament diameter 1.75 mm is used. The one, two and four layers microchannels are manufactured with a 0.2 mm nozzle to obtain thin walls that provide better sound absorption [11]. The printing speed is set at 27 mm/s. The extrusion temperature is set at 235°C to avoid nozzle clogging. The bed temperature is set at 50°C. All microchannels are produced using the "Zigzag" 3D printing pattern [13]. Figure 4a shows a schematic of the Zigzag 3D printing pattern and Figure 4b to d show pictures of 3D printed samples. The channels

are produced via deposition of filaments along the zig-zag trajectory illustrated by the white points (p_1, p_2, …, p_n) and arrows (Figure 4a and c). The FFF Zigzag 3D printing pattern is implemented in Matlab R2019a. The Zigzag 3D printing pattern produces microchannels without transverse porosity (i.e., interconnections between channels) [13]. Figure 4b shows a picture of a sample 3D printed with the optimal parameters of

Table I. Close contact at corners (Figure 4c) and adjusted printing layer height (i.e., 0.1mm) prevent having voids in the walls. Figure 4d shows clearly that the walls of the microchannels are completely sealed and exhibit no apparent transverse porosities. The sealed walls avoid air diffusion between channels and improve the mechanical properties [13]. On the contrary, the standard 3D printing pattern to create microchannels would be the grid infill pattern commonly used by 3D printers. The grid 3D printing pattern consists of successive deposition of orthogonal filaments overlapping each other with the same layer height. However, due to overlapping at filament intersections, transverse porosity appears, leading to voids in the walls, and therefore undesired interconnections between microchannels.

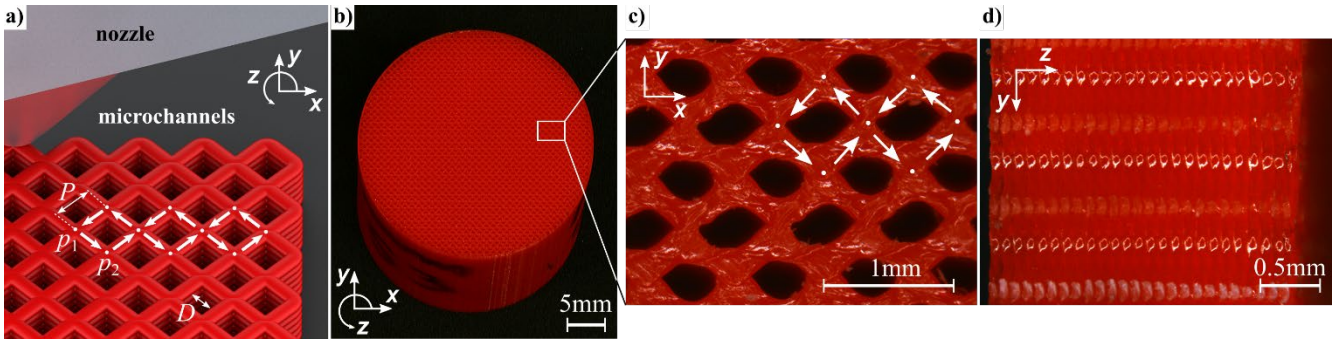

Figure 4 – Manufacturing of 1 layer microchannels: a) schematic of the Zigzag 3D printing pattern; b) sample 3D printed with the optimal parameters of

Table **I**. c) Optical microscopy images of the top of the sample (32× magnification) and d) the walls (50× magnification).

Figure 5 illustrates the manufacturing of 2 and 4 layers microchannels with the Zigzag 3D printing pattern. In order to print small channels over bigger ones, supports are added as shown in Figure 5a. The support filaments rest on the edges of the samples and on the walls of the previously printed channels. Additionally, to avoid obstruction of the microchannels, the support filaments are aligned with the walls of the channels they will support. Figure 5b shows the interior of a 30 mm thick sample of 4 layers microchannels with the characteristics described in

Table I. Figure 5c shows in detail the transition between the 4.6 mm channels (at the bottom of the figure) and 0.1 mm microchannels (at the top). The two dashed lines on Figure 5c indicate the alignment of the supports with the walls of the 0.1 mm microchannels. The Zigzag 3D printing pattern enables the manufacturing of microchannels with 0.1 mm minimum size. Such small perforations are difficult to obtain with conventional manufacturing techniques, but it is required for acoustic liners or micro-perforated panels with optimal sound absorption [12,13,38]. The Zigzag 3D printing pattern can produce acoustic liners with multiple degrees of freedom in one manufacturing step, thus avoiding any subsequent parts assembly. Microchannels treatment with the thickness and the pore size presented in this work cannot be obtained via Stereolithography (SLA) because the laser beam polymerizes resin in the surroundings of the desired areas. Therefore, removing the resin from inside the microchannels is difficult. This issue was also raised in [16] during the manufacturing of structures with triply periodic minimal surfaces (TPMS).

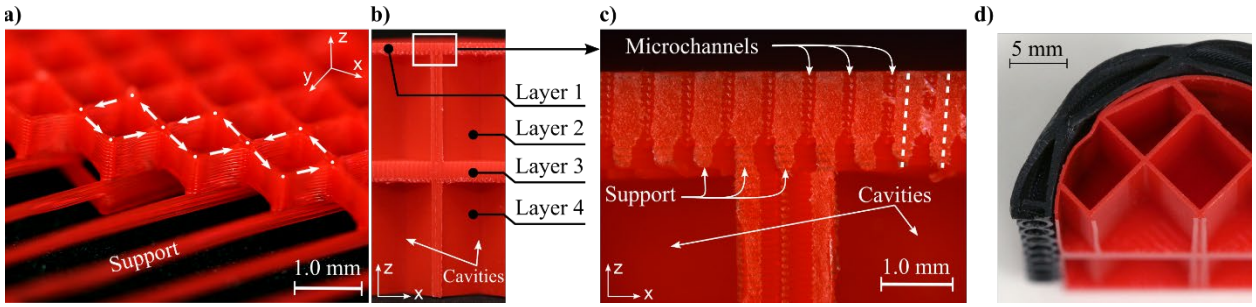

Figure 5 – Manufacturing of 2 and 4 layers microchannels: a) detail of the supports used to print small channels over bigger ones; b) interior of a cut 30 mm thick acoustic sample with 4 layers; c) detail of the transition between 4.6 mm and 0.1 mm microchannels; d) detail of the bottom part of a sample.

The coiled tubes are designed in CATIA version 5-6 Release 2018 with straight line, helix and spline curves as well as the rib and circular pattern tools. The CATPart files are exported in STL files which are sliced with the Simplify3D software. The printing layer heights of the structures with $N = 7$ ($\xi = 1.25$); $N = 5$ ($\xi = 1.75$); $N = 3$ ($\xi = 2.95$) are set at 0.1 mm, 0.05 mm, 0.03 mm, respectively. The printing layer height for the tubes with higher number of rotations is lower to avoid porosity in the walls of the tubes. The printing speed of the tubes is set at 35 mm/s and the extrusion and bed temperatures are set at 210°C and 50°C, respectively. The internal diameter formed by the coiled tubes is designed to receive cylindrical microchannel part. After 3D printing the tubes and microchannels, the two parts are assembled manually by tight fitting to form the hybrid material. There is no opening between the helix tubes and the cavities or micro-channels. The resulting assembly has a total diameter of 30 mm that fits the impedance tube. All samples are 30 mm thick.

Nine hybrid materials are studied in this work. They are combinations of microchannels with 1, 2 and 4 layers and coiled tubes with $N = 7$, 5 and 3. The parameters of the microchannels and the coiled tubes are described in

Table I and Table II. Table III shows the calculated and the measured tube length L. The tube length is measured by means of flexible filament runing from one end of the tube to the other end. The length of flexible filament is measured afterwards with a simple ruler. The experimental error between the measured and the calculated values does not exceed 2%.

Table III – Calculated and measured tube length L

Number of tubes (N)	**Number of rotations (ξ)**	**Calculated tube length, L**	**Measured tube length, L**	**Deviation**
7	1.25	110 mm	109 mm	0.91%
5	1.75	151 mm	150 mm	0.66%
3	2.95	250 mm	250 mm	0%

Acoustic characterization

Figure 6 shows a schematic of the impedance tube used to obtain the experimental sound absorption coefficient. The impedance tube is equipped with two microphones in absorption configuration – i.e. hard backing behind the sample – according to ASTM E1050 [39] and ISO 10534-2 [40] standards. All measurements are performed in the 500-4000 Hz frequency range. The sound pressure level is 94 dB. The sound absorption coefficient (α) in octave bands centered at 500 Hz (α_{500}) and 1000 Hz (α_{1000}) are used to compare the structures. α_{500} and α_{1000} are the averages of the narrow band (step of 1 Hz) sound absorption coefficient for the frequency ranges 355-710 Hz and 710-1420 Hz, respectively [41].

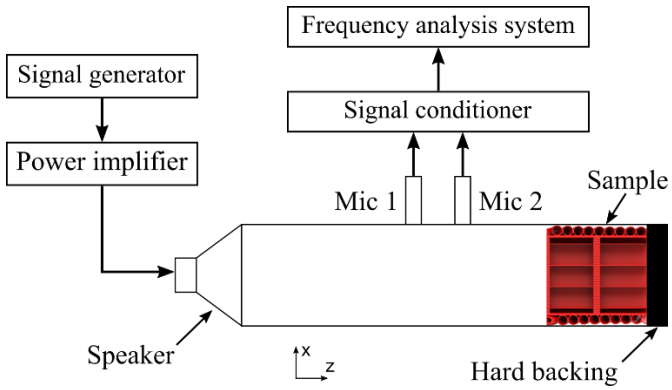

Figure 6 – Measurement set-up with the 30 mm diameter impedance tube [8].

Results and discussions

Microstructure of 3D printed hybrid materials

Figure 7a-c show images of the hybrid materials with 4 layers microchannels and 7, 5 and 3 tubes, respectively. Figure 8 shows a picture of the internal cross section of the produced sample. Such hybrid material with long coiled tubes and microchannels with 100 µm perforations could hardly be produced with conventional fabrication methods. The hybrid material with microchannels contains air cavities and requires small amount of material. Therefore, it is a low cost and lightweight solution for noise control. Moreover, it can be noticed that the manufactured structure is consistent with the designed one demonstrating the capability of the FFF 3D printing to reproduces functional structures for noise absorption. A small gap between the circular coiled tubes and the microchannels is observed in Figure 8c. This leads to the formation of an additional 'coiled volume' as shown by the white arrow. This gap may contribute to the overall acoustic performance of the material. The results from the experimental acoustic characterization of the hybrid materials are presented and discussed in the next sections.

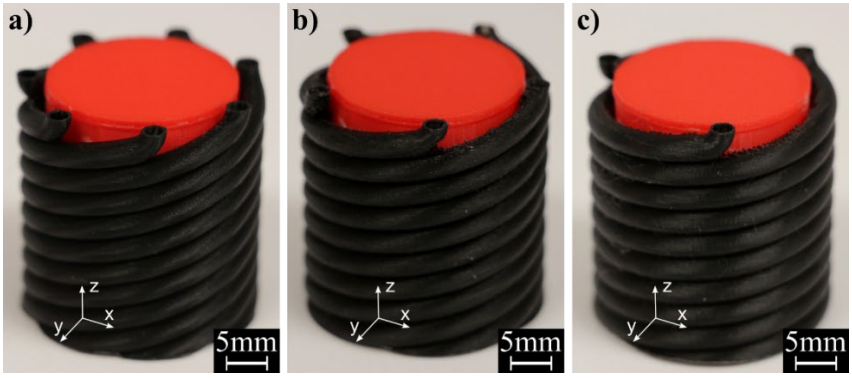

Figure 7 – Assembled hybrid materials with 4 layers microchannels and: a) 7 tubes; b) 5 tubes; c) 3 tubes.

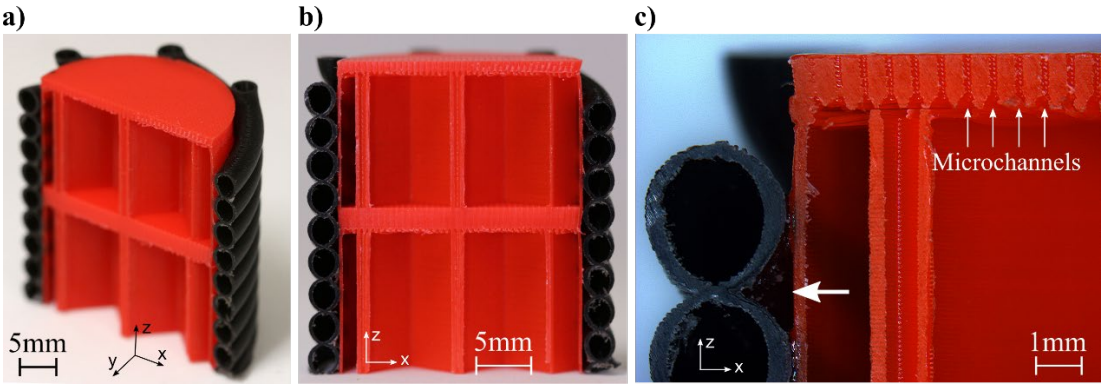

Figure 8 – Pictures of the internal structure of the hybrid material with 4-layers microchannels and 7 tubes: a) Perspective view of the assembly b) Front view c) Detail of the upper left of the sample.

Sound absorption characterization

Materials with coiled tubes and 1-layer microchannels

Figure 9a presents the sound absorption coefficient of the assembled materials composed of 0, 3, 5 and 7 coiled tubes and one layer of microchannels. The black curve with circular marker is the absorption of 1 layer microchannels without tubes. Table **IV** lists the number of rotations ξ, the frequency f_1 and absorption coefficient α_1 of the first absorption peak, the wavelength ratio λ_1/T, α_{500} and α_{1000} of the 4 structures. For all hybrid materials, the first absorption peaks are lower than the one corresponding to 1 layer microchannels without tubes. This is evidence that the presence of coiled tubes shifts the absorption towards lower frequencies and improves the acoustic performance. For instance, α_{500} for the 7, 5 and 3 tubes is ~1.56, 2.11, 3.78 times higher than α_{500} for zero tubes and 1 layer microchannels, respectively. Moreover, α_{1000} is ~ 1.54, 1.94, and 1.03 times higher for the materials with 1 layer and 7, 5 and 3 tubes than for the 1 layer microchannel material without tubes, respectively. α_{1000} is lower for the 3 tubes structure than for the 7 and 5 tubes due to the valley between the first and second absorption peaks. The first absorption peak of the structure with the three tubes is located at the lowest frequency (~ 600Hz). Since the material thickness is kept constant (T = 30mm), λ_1/T increases progressively from

5.0 for the 1 layer microchannels to a deep sub-wavelength with λ_1/T ~17 for the hybrid material with 3 coiled tubes.

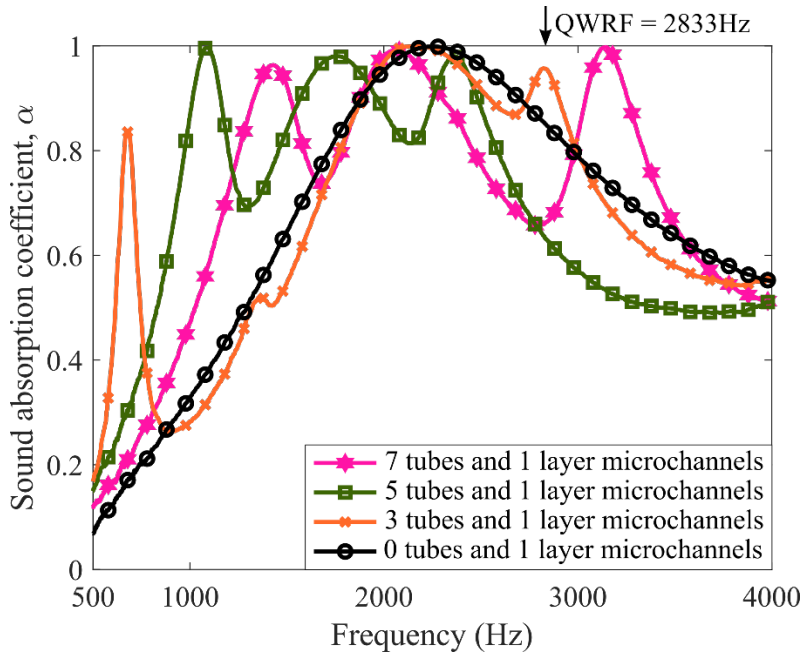

Figure 9 – Absorption coefficient of hybrid material with 1 layer microchannels and N = 0, 3, 5 and 7

Table IV – Number of rotations $\boldsymbol{\xi}$, frequency $\boldsymbol{f_1}$ and absorption coefficient $\boldsymbol{\alpha_1}$ of the first absorption peak, wavelength ratio $\boldsymbol{\lambda_1/T}$, $\boldsymbol{\alpha_{500}}$ and $\boldsymbol{\alpha_{1000}}$ of the structures with 1 layer microchannels

	$\boldsymbol{\xi}$	$\boldsymbol{f_1}$ **(Hz)**	$\boldsymbol{\alpha_1}$	$\boldsymbol{\lambda_1/T}$	$\boldsymbol{\alpha_{500}}$	$\boldsymbol{\alpha_{1000}}$
1-layer	-	2260	1.0	5.0	0.09	0.37
1 layer + 7 tubes	1.25	1429	0.96	7.9	0.14	0.57
1 layer + 5 tubes	1.75	1090	1.0	10.4	0.19	0.72
1 layer + 3 tubes	2.95	680	0.83	16.7	0.34	0.38

Hybrid material with coiled tubes and microchannels

Figure 10 and Figure 11 present the sound absorption coefficient of hybrid materials composed of 0, 3, 5, and 7 coiled tubes and microchannels. For comparison purposes, the absorption of microchannel is shown on the same graph. ξ, f_1, α_1, λ_1/T, α_{500} and α_{1000} of the hybrid materials with 2 and 4 layers microchannels are listed in Table V. As in the previous case, the assembled materials present absorption peaks below the one of the microchannels. However, the improvement at low frequencies is less significant. This is due to the fact that 2 and 4 layers microchannels already present better absorption

than 1 layer microchannels at lower frequencies. α_{500} is ~1.35, 1.58, 2.00 times higher for the materials with 2 layers and 7, 5 and 3 tubes than for the 2 layers microchannel material without tubes, respectively. Alternatively, the α_{1000} of the structures with 7, 5 and 3 tubes are ~1.23, 1.18, and 1.10 times higher than the α_{1000} of 2 layers microchannels without tubes, respectively. The 4 layers microchannels present equivalent results. Regardless of the nature of the microchannels, the length of the coiled tubes can be further augmented by increasing the surface of the treatment according to Eqs. (1) and (2). For instance, the length of the tubes of a material with 2 tubes and 5.0 mm of diameter can reach 50 cm if the diameter of the porous material is changed from 30 mm to 100 mm. The absorption frequency peak would be decrease from 680 Hz to 300 Hz. The developed hybrid materials are relatively inexpensive and can be applied in scenarios where combining low frequency noise reduction to weight and volume constraints is challenging. Some examples are the transport industry in general (i.e., aircrafts, automobiles and trains), ventilation and cooling systems. Other possible application is the improvement of the acoustic insulation and quality of nightclubs, classrooms and concert halls. The hybrid structures are produced using PLA material. However, if the same geometry (i.e., identical pore size, wall thickness and surface finish) is reproduced with other materials (e.g., ABS or reinforced polymers), identical acoustic behavior should be obtained.

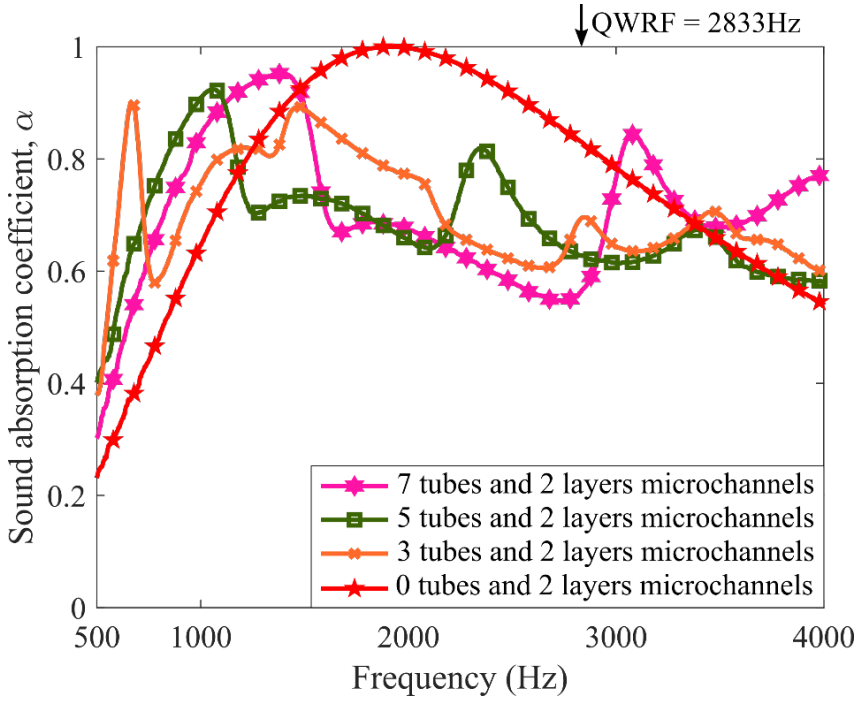

Figure 10 – Absorption coefficient of hybrid material with 2 layers microchannels and N = 0, 3, 5 and 7

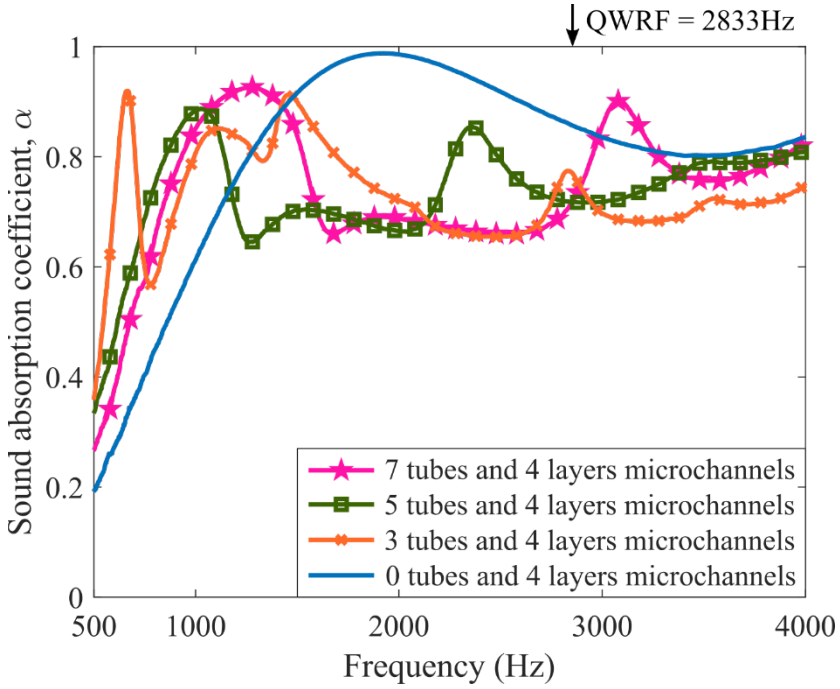

Figure 11 – Absorption coefficient of hybrid material with 4 layers microchannels and N = 0, 3, 5 and 7

Table V – $\boldsymbol{\xi}$, $\boldsymbol{f_1}$, $\boldsymbol{\alpha_1}$, $\boldsymbol{\lambda_1/T}$, $\boldsymbol{\alpha_{500}}$ and $\boldsymbol{\alpha_{1000}}$ of the structures with 2 layers microchannels

	$\boldsymbol{\xi}$	$\boldsymbol{f_1}$ (Hz)	$\boldsymbol{\alpha_1}$	$\boldsymbol{\lambda_1/T}$	$\boldsymbol{\alpha_{500}}$	$\boldsymbol{\alpha_{1000}}$
2 layers	-	1910	1.0	5.9	0.26	0.68
7 tubes + 2 layers	1.25	1400	0.95	8.1	0.35	0.84
5 tubes + 2 layers	1.75	1060	0.92	10.7	0.41	0.80
3 tubes + 2 layers	2.95	668	0.89	17	0.52	0.75
4 layers	-	1920	0.99	5.9	0.22	0.65
7 tubes + 4 layers	1.25	1268	0.93	8.9	0.32	0.82
5 tubes + 4 layers	1.75	1029	0.89	11	0.38	0.76
3 tubes + 4 layers	2.95	665	0.91	17	0.50	0.76

Conclusions

In this work, proof-of-concept of sound absorbing hybrid materials made of parallel assembly of coiled tubes and a network of straight microchannels is presented. A manufacturing procedure based on fused filament deposition is used to produce submillimeter size microchannels. The 3D printed coiled tubes and the microchannels are assembled by tight fitting the two pieces together. Although the manufacturing procedure can be improved to avoid the assembly step, the creation of this hybrid material would hardly be achievable with conventional manufacturing techniques. The experimental analyses showed that the

type of microchannels (i.e., one, two or four layers), the number of tubes and number of rotations are key parameters to improve the low frequency sound absorption. The sound absorption coefficient in the 500Hz octave band (α_{500}) increases from 0.09 to 0.52 without increasing the treatment thickness. The assembled material exhibits deep-subwavelength behavior and broadband sound absorption. In fact, the first peak wavelength to material thickness ratio λ_1/T reaches 17 with octave-band absorption coefficients above 0.5 (i.e., $\alpha_{500} > 0.5$ and $\alpha_{1000} > 0.7$). The proposed material shows that low frequency acoustic absorption can be achieved without increasing the thickness of the material.

REFERENCES

[1] M. Askari, D.A. Hutchins, P.J. Thomas, L. Astolfi, R.L. Watson, M. Abdi, M. Ricci, S. Laureti, L. Nie, S. Freear, R. Wildman, C. Tuck, M. Clarke, E. Woods, A.T. Clare, Additive manufacturing of metamaterials: A review, Addit. Manuf. 36 (2020) 101562. https://doi.org/10.1016/j.addma.2020.101562.

[2] T. Sathies, P. Senthil, M.S. Anoop, A review on advancements in applications of fused deposition modelling process, Rapid Prototyp. J. 26 (2020) 669–687. https://doi.org/10.1108/RPJ-08-2018-0199.

[3] M. Sauerwein, E. Doubrovski, R. Balkenende, C. Bakker, Exploring the potential of additive manufacturing for product design in a circular economy, J. Clean. Prod. 226 (2019) 1138–1149. https://doi.org/10.1016/j.jclepro.2019.04.108.

[4] Y. Tang, Y.F. Zhao, A survey of the design methods for additive manufacturing to improve functional performance, Rapid Prototyp. J. 22 (2016) 569–590. https://doi.org/10.1108/RPJ-01-2015-0011.

[5] J.C. Najmon, S. Raeisi, A. Tovar, Review of additive manufacturing technologies and applications in the aerospace industry, Addit. Manuf. Aerosp. Ind. (2019) 7–31. https://doi.org/10.1016/B978-0-12-814062-8.00002-9.

[6] A. Merulla, A. Gatto, E. Bassoli, S.I. Munteanu, B. Gheorghiu, M.A. Pop, T. Bedo, D. Munteanu, Weight reduction by topology optimization of an engine subframe mount, designed for additive manufacturing production, Mater. Today Proc. 19 (2019) 1014–1018. https://doi.org/10.1016/j.matpr.2019.08.015.

[7] C. Li, D. Pisignano, Y. Zhao, J. Xue, Advances in Medical Applications of Additive Manufacturing, Engineering. 6 (2020) 1222–1231. https://doi.org/10.1016/j.eng.2020.02.018.

[8] E.R. Fotsing, A. Dubourg, A. Ross, J. Mardjono, Acoustic properties of periodic micro-structures obtained by additive manufacturing, Appl. Acoust. 148 (2019) 322–331. https://doi.org/10.1016/j.apacoust.2018.12.030.

[9] T.G. Zieliński, K.C. Opiela, P. Pawłowski, N. Dauchez, T. Boutin, J. Kennedy, D. Trimble, H. Rice, B. Van Damme, G. Hannema, R. Wróbel, S. Kim, S. Ghaffari Mosanenzadeh, N.X. Fang, J. Yang, B. Briere de La Hosseraye, M.C.J. Hornikx, E. Salze, M.-A. Galland, R. Boonen, A. Carvalho de Sousa, E. Deckers, M. Gaborit, J.-P. Groby, Reproducibility of sound-absorbing periodic porous materials using additive manufacturing technologies: Round robin study, Addit. Manuf. 36 (2020) 101564. https://doi.org/10.1016/j.addma.2020.101564.

[10] J. Boulvert, J. Costa-Baptista, T. Cavalieri, M. Perna, E.R. Fotsing, V. Romero-García, G. Gabard, A. Ross, J. Mardjono, J.-P. Groby, Acoustic modeling of micro-lattices obtained by additive manufacturing, Appl. Acoust. 164 (2020) 107244.

https://doi.org/10.1016/j.apacoust.2020.107244.
[11] J. Boulvert, T. Cavalieri, J. Costa-Baptista, L. Schwan, V. Romero-García, G. Gabard, E.R. Fotsing, A. Ross, J. Mardjono, J.-P. Groby, Optimally graded porous material for broadband perfect absorption of sound, J. Appl. Phys. 126 (2019) 175101. https://doi.org/10.1063/1.5119715.
[12] J.C. Baptista, E. Roland-Fotsing, J. Mardjano, D. Therriault, A. Ross, Multilayer treatment for subwavelength and broadband absorption, in: INTER-NOISE NOISE-CON Congr. Conf. Proc., Institute of Noise Control Engineering, 2021: pp. 2219–2227. https://www.researchgate.net/publication/358622964_Multilayer_treatment_for_subwavelength_and_broadband_absorption.
[13] J. Costa-Baptista, E.R. Fotsing, J. Mardjono, D. Therriault, A. Ross, Design and fused filament fabrication of multilayered microchannels for subwavelength and broadband sound absorption, Addit. Manuf. 55 (2022) 102777. https://doi.org/10.1016/j.addma.2022.102777.
[14] J. Costa-Baptista, E.-R. Fotsing, J. Boulvert, J. Mardjono, D. Therriault, A. Ross, Sonic crystal acoustic absorbers produced by fugitive ink, in: 1st Aerosp. Eur. Conf., Bordeaux, 2020: p. 8. https://www.researchgate.net/publication/354682278_Characterization_of_sonic_crystal_acoustic_absorbers_produced_by_fugitive_ink_manufacturing_process.
[15] N. Gao, H. Hou, Sound absorption characteristic of micro-helix metamaterial by 3D printing, Theor. Appl. Mech. Lett. 8 (2018) 63–67. https://doi.org/10.1016/j.taml.2018.02.001.
[16] W. Yang, J. An, C.K. Chua, K. Zhou, Acoustic absorptions of multifunctional polymeric cellular structures based on triply periodic minimal surfaces fabricated by stereolithography, Virtual Phys. Prototyp. 15 (2020) 242–249. https://doi.org/10.1080/17452759.2020.1740747.
[17] G. do N. Almeida, E.F. Vergara, L.R. Barbosa, A. Lenzi, R.S. Birch, A low-frequency sound absorber based on micro-slit and coiled cavity, J. Brazilian Soc. Mech. Sci. Eng. 43 (2021) 1–9. https://doi.org/10.1007/s40430-020-02763-y.
[18] A. Arjunan, Acoustic absorption of passive destructive interference cavities, Mater. Today Commun. 19 (2019) 68–75. https://doi.org/10.1016/j.mtcomm.2018.12.012.
[19] F. Setaki, M. Tenpierik, M. Turrin, A. van Timmeren, Acoustic absorbers by additive manufacturing, Build. Environ. 72 (2014) 188–200. https://doi.org/10.1016/j.buildenv.2013.10.010.
[20] J. Boulvert, J. Costa-Baptista, T. Cavalieri, V. Romero-García, G. Gabard, E.R. Fotsing, A. Ross, M. Perna, J. Mardjono, J.-P. Groby, Folded metaporous material for sub-wavelength and broadband perfect sound absorption, Appl. Phys. Lett. 117 (2020) 251902. https://doi.org/10.1063/5.0032809.
[21] D.L. Johnson, J. Koplik, R. Dashen, Theory of dynamic permeability and tortuosity in fluid-saturated porous media, J. Fluid Mech. 176 (1987) 379. https://doi.org/10.1017/S0022112087000727.
[22] Y. Champoux, J. Allard, Dynamic tortuosity and bulk modulus in air-saturated porous media, J. Appl. Phys. 70 (1991) 1975–1979. https://doi.org/10.1063/1.349482.
[23] D. Lafarge, P. Lemarinier, J.F. Allard, V. Tarnow, Dynamic compressibility of air in porous structures at audible frequencies, J. Acoust. Soc. Am. 102 (1997) 1995–2006. https://doi.org/10.1121/1.419690.
[24] J.F. Allard, N. Atalla, Propagation of Sound in Porous Media: Modelling Sound Absorbing Materials, 2nd ed., John Wiley & Sons, Ltd, Chichester, UK, 2009. https://doi.org/10.1002/9780470747339.
[25] N. Atalla, F. Sgard, Modeling of perforated plates and screens using rigid frame porous models, J. Sound Vib. 303 (2007) 195–208. https://doi.org/10.1016/j.jsv.2007.01.012.
[26] J.-L. Auriault, C. Boutin, C. Geindreau, Homogenization of Coupled Phenomena in Heterogenous Media, ISTE, London, UK, 2009. https://doi.org/10.1002/9780470612033.

[27] J.A. Nelder, R. Mead, A Simplex Method for Function Minimization, Comput. J. 7 (1965) 308–313. https://doi.org/10.1093/comjnl/7.4.308.
[28] J. D'Errico, Bound constrained optimization using fminsearch, MATLAB Cent. File Exch. (2010). http://www.mathworks.com/matlabcentral/fileexchange/8277-fminsearchbnd.
[29] J. Costa-Baptista, E.R. Fotsing, J. Boulvert, J. Mardjono, D. Therriault, A. Ross, Design and fused filament fabrication of microchannels with high broadband sound absorption, Appl. Acoust. (2022) Under review.
[30] H. Guo, Y. Wang, X. Wang, C. Xu, Investigation on acoustic energy harvesting based on quarter-wavelength resonator phononic crystals, Adv. Mech. Eng. 10 (2018) 1687814017748077. https://doi.org/10.1177/1687814017748077.
[31] A. Bastida, J. Zúñiga, A. Requena, B. Miguel, J. Cerezo, On the Role of Entropy in the Stabilization of α-Helices, J. Chem. Inf. Model. 60 (2020) 6523–6531. https://doi.org/10.1021/acs.jcim.0c01177.
[32] M.C. Parker, C. Jeynes, Maximum Entropy (Most Likely) Double Helical and Double Logarithmic Spiral Trajectories in Space-Time, Sci. Rep. 9 (2019) 1–10. https://doi.org/10.1038/s41598-019-46765-w.
[33] G. Lester, R. Kamien, Why Is The Helix Such A Popular Shape? Perhaps Because They Are Nature's Space Savers, Sci. Dly. (2005) 2. https://penntoday.upenn.edu/news/why-helix-such-popular-shape-perhaps-because-they-are-natures-space-savers (accessed June 7, 2022).
[34] Y. Snir, R.D. Kamien, Entropically Driven Helix Formation, Science (80-.). 307 (2005) 1067–1067. https://doi.org/10.1126/science.1106243.
[35] A. Sheeba, P. Mathew, P.M. Jose, Numerical investigations on the heat transfer characteristics of tube in tube helical coil heat exchanger, J. Phys. Conf. Ser. 1355 (2019) 490–497. https://doi.org/10.1088/1742-6596/1355/1/012005.
[36] A. Baratta, I. Corbi, Equilibrium models for helicoidal laterally supported staircases, Comput. Struct. 124 (2013) 21–28. https://doi.org/10.1016/j.compstruc.2012.11.007.
[37] F.F. Calim, Y.C. Cuma, Forced vibration analysis of viscoelastic helical rods with varying cross-section and functionally graded material, Mech. Based Des. Struct. Mach. (2021) 1–12. https://doi.org/10.1080/15397734.2021.1931307.
[38] D.-Y. Maa, Potential of microperforated panel absorber, J. Acoust. Soc. Am. 104 (1998) 2861–2866. https://doi.org/10.1121/1.423870.
[39] ASTM International, ASTM E1050−12: Standard Test Method for Impedance and Absorption of Acoustical Materials Using a Tube, Two Microphones and a Digital Frequency Analysis System, (2012). https://doi.org/https://doi.org/10.1520/D0695-15.
[40] ISO, 10534–2: Acoustics—Determination of Sound Absorption Coefficient and Impedance in Impedance Tubes—Part 2: Transfer-Function Method., 1998.
[41] S. Errede, Center frequencies and high/low frequency limits for octave bands, 1/2- and 1/3-octave bands, Phys. 406 Course Univ. Illinois Urbana-Champaign. (2017) 3. https://courses.physics.illinois.edu/phys406/sp2017/Lab_Handouts/Octave_Bands.pdf (accessed November 13, 2021).